Liver-Target and Glucose-Responsive Polymersomes toward Mimicking Endogenous Insulin Secretion with Improved Hepatic Glucose Utilization

Aohua Wang, Weiwei Fan, Tiantian Yang, Shufang He, Yiwei Yang, Miaorong Yu, Li Fan, Quanlei Zhu, Shiyan Guo, Chunliu Zhu, and Yong Gan*

Oral insulin therapy that targets the liver and further mimics glucose-responsive secretion holds promise for correcting defects in glucose metabolism caused by peripheral delivery. This work describes the construction of polymersomes (Pep-PMS), which are composed of glucose-responsive polymers decorated with peptides that readily bind to the ganglioside-monosialic acid (GM1) receptor in the intestinal epithelium. Pep-PMS are efficiently transported across the intestinal epithelium through GM1-mediated transcytosis, leading to their abundant accumulation in the liver. Moreover, Pep-PMS can efficiently encapsulate insulin in euglycemia and release them in hyperglycemia. Under hyperglycemic conditions, the Pep-PMS dissociate to release the encapsulated insulin in response to glucose oxidase (GOx)-induced H_2O_2. Surprisingly, the postprandial blood glucose levels of diabetic rats treated with Pep-PMS can be maintained even after being challenged by glucose administration. Hepatic glucose uptake and glycogen production are also elevated after treating diabetic rats with Pep-PMS, which is similar to glucose utilization in normal rats. Oral delivery systems that target the liver and serve as a reservoir for glucose-responsive insulin secretion may improve the therapeutic effect in people with diabetes.

1. Introduction

Diabetes mellitus is the most prevalent chronic metabolic disease worldwide, with 425 million people suffering from it in

A. H. Wang, Dr. W. W. Fan, T. T. Yang, Dr. S. F. He, Y. W. Yang,
Dr. M. R. Yu, Dr. Q. L. Zhu, S. Y. Guo, Dr. C. L. Zhu, Prof. Y. Gan
Center for Pharmaceutics Research
Shanghai Institute of Materia Medica
Chinese Academy of Sciences
Shanghai 201203, China
E-mail: ygan@simm.ac.cn
A. H. Wang, Dr. W. W. Fan, T. T. Yang, Dr. S. F. He, Y. W. Yang, Prof. Y. Gan
School of Pharmacy
University of Chinese Academy of Sciences
Beijing 10049, China
Dr. L. Fan
Novo Nordisk Research Centre China
Building 2
No. 20 Life Science Park Road, Changping District
Beijing 102206, China

The ORCID identification number(s) for the author(s) of this article can be found under https://doi.org/10.1002/adfm.201910168.

2017.[1] For type I and advanced type II diabetic patients, the administration of exogenous insulin is the only therapy. However, exogenous insulin administration is different from endogenously secreted insulin with respect to the physiological portal-to-peripheral gradient, leading to peripheral hyperinsulinemia. Under physiological conditions, the glucose absorbed after digestion of food leads to elevated postprandial blood glucose levels, and immediately in response to this, insulin is secreted from pancreatic β cells.[2] After entering the liver through the portal vein, insulin mostly accumulates in the liver to stimulate glucose intake and glycogenesis. Furthermore, this insulin is released into the blood circulation with proper acting concentration through the liver, thus resulting in a much higher concentration than that in the peripheral tissues.[3] This portal-to-peripheral insulin gradient ensures the control of postprandial blood glucose levels without side effects.[4] Moreover, the synthesized hepatic glycogen is responsible for the maintenance of normoglycemia between meals. As reported, subcutaneous injection of insulin cannot resolve the defect in postprandial hepatic glycogen storage in type I diabetic patients.[5] Oral delivery of exogenous insulin is preferred and promising because it can simulate the biodistribution of endogenous insulin, which satisfies the high portal-to-peripheral gradient. So far, many nanocarriers such as liposomes, nanoparticles, and polymersomes (PMS) have been developed to improve the oral absorption of insulin.[6] Although the hypoglycemic effect has been achieved, these conventional nanocarriers cannot respond to blood glucose fluctuations, i.e., they cannot repeatedly exert their hypoglycemic potency. Meanwhile, it is extremely important for exogenous insulin to take effect only under hyperglycemic conditions. Therefore, it may be promising to deliver an insulin reservoir to the liver via oral route and release preloaded insulin in a glucose-responsive manner, mimicking the endogenous hypoglycemic mechanisms through insulin and ameliorating the glucose utilization in the liver.

The intestinal epithelium is the most formidable barrier limiting the oral absorption of insulin. In contrast, over a long period of symbiosis between microbes and humans,

some pathogenic bacteria have found several pathways to deliver toxins across the intestinal epithelium.[7] Among them, cholera toxin subunit B (CTB) has been reported to be transported across the intestinal epithelium through the ganglioside GM1-mediated transcytosis pathway.[8] After binding to GM1 in the apical membrane, CTB can be internalized and then transferred to the Golgi apparatus from the endosome via a retrograde pathway, thus bypassing lysosomes and avoiding lysosomal degradation. Finally, CTB moves to the basolateral membrane to facilitate exocytosis.[9] Inspired from this, a GM1-targeted nanocarrier may efficiently overcome the intestinal epithelium barrier.

To acquire glucose-dependent release properties, insulin carriers are fabricated to typically incorporate glucose-sensing components such as glucose oxidase (GOx), glucose-binding proteins, or phenylboronic acids to regulate the release rate of insulin by polymer degradation, structure switching, or glucose-binding competition.[10] GOx has been extensively used because of its catalytic conversion of glucose to gluconic acid, resulting in a lower pH, hypoxia, and increased concentration of H_2O_2.[11] As recently reported, many functional polymers have been synthesized that can respond to GOx-induced hypoxia and abundant H_2O_2, leading to satisfactory glucose-responsive insulin release from the delivery systems.[12] Because the intestinal environment is highly associated with hypoxia and varying pH, to avoid destroying the systems before absorption, designing nanocarriers sensitive to H_2O_2 may provide a glucose-responsive function that is applicable for oral delivery.[13]

Here, we developed smart PMS (Pep-PMS) that can accumulate in the liver after oral administration and release insulin in a glucose-responsive manner (**Scheme 1**). We introduced a GM1-targeting peptide screened from a phage library into the PMS to overcome the intestinal epithelium barrier.[14] After accumulation in the liver, Pep-PMS could release insulin under hyperglycemic conditions due to the oxidation of the

polymer by the high H_2O_2 levels induced by GOx. In vivo pharmacodynamics (PD) studies showed that Pep-PMS could substantially reduce the blood glucose level; especially, when this level is elevated due to food intake, the loaded insulin could again be released in the liver to regulate postprandial blood glucose levels. Furthermore, on treating diabetic rats with Pep-PMS, glucose uptake in the liver was found to be elevated and more hepatic glycogen was produced. This work demonstrates that developing smart oral delivery systems that can mimic the glucose-responsive secretion of endogenous insulin is a promising alternative to the current insulin therapy. Most importantly, we provide a biomimetic strategy widely applicable for all insulin delivery systems to improve glycemic control for diabetes treatment.

2. Results

2.1. Synthesis and Characterization of Functional Polymers

2.1.1. Synthesis and Characterization of mPEG-PolyMet

Polymers that contain sulfide bond can respond to H_2O_2. Thus, the sulfide bond-containing diblock copolymer mPEG-PolyMet was first synthesized by amine-initiated ring-opening polymerization of α-methionine-N-carboxyanhydride (Met-NCA; **Figure 1**a). It is reported that such type of polymer composed of poly(amino acids) and polyethylene glycol (PEG) has good biocompatibility and biodegradability.[12c,15] The synthesis of Met-NCA from methionine was confirmed by ^1H and ^{13}C NMR spectroscopy (Figure S1, Supporting Information). Then, after polymerization, the characteristic peaks of mPEG and Met in the ^1H NMR spectrum of the isolated product were observed (Figure 1b), demonstrating the successful synthesis of mPEG-PolyMet. The molecular weight of mPEG-PolyMet measured by gel permeation chromatography (GPC) was found to be 5917 g mol^{-1} with a narrow distribution (Figure S2, Supporting Information). The structural changes of mPEG-PolyMet after incubation with H_2O_2 were confirmed by Fourier transform infrared spectroscopy (FTIR), and stretching vibrations of sulfone moieties at ≈1033 cm^{-1} were observed (Figure 1e).[16] These results demonstrated that the synthesized mPEG-PolyMet exhibited H_2O_2-sensitivity. To evaluate the minimum H_2O_2 concentrations to induce the oxidation of mPEG-PolyMet, the absorbance of Pep-PMS through self-assembly of polymer at 500 nm in the presence of different H_2O_2 concentrations was recorded. As shown in Figure S3 in the Supporting Information, no obvious changes in the absorbance were observed when the H_2O_2 concentration was low. As the H_2O_2 concentration increased to 25×10^6 M, a larger change in absorbance was observed. This demonstrated that the minimum H_2O_2 concentration to oxidize mPEG-PolyMet was 25×10^6 M. To further investigate the integrity of the polymer chain, ^1H-NOESY was performed as reported previously.[16b] The cross-peaks between PEG and other protons were observed both before and after H_2O_2 incubation. Combined with the result that the same chemical bonds existed in the FTIR spectra after incubation (Figure 1e), these results confirmed that the product of mPEG-PolyMet left the chain substantially intact (Figure S4, Supporting Information). Moreover,
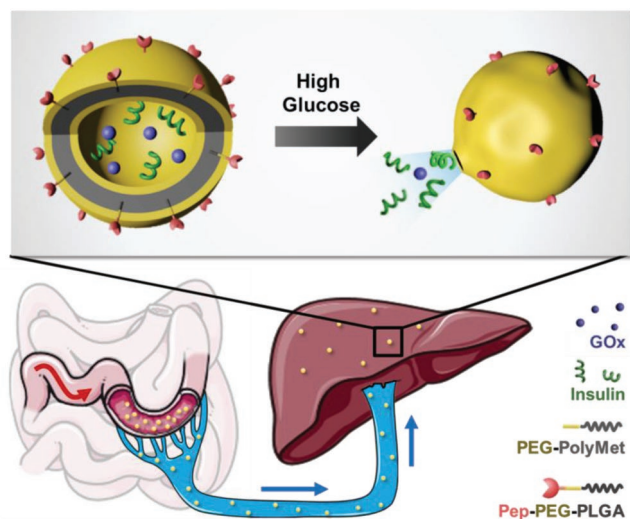
Scheme 1. Illustration of Pep-PMS traversing the intestinal epithelium, accumulating in the liver, and releasing insulin in response to elevated blood glucose levels. GOx, glucose oxidase. PEG-PolyMet, methoxypolyethylene glycol-polymethionine. Pep-PEG-PLGA, ganglioside GM1-targeting peptide-modified PEG-poly (lactide-co-glycolide).
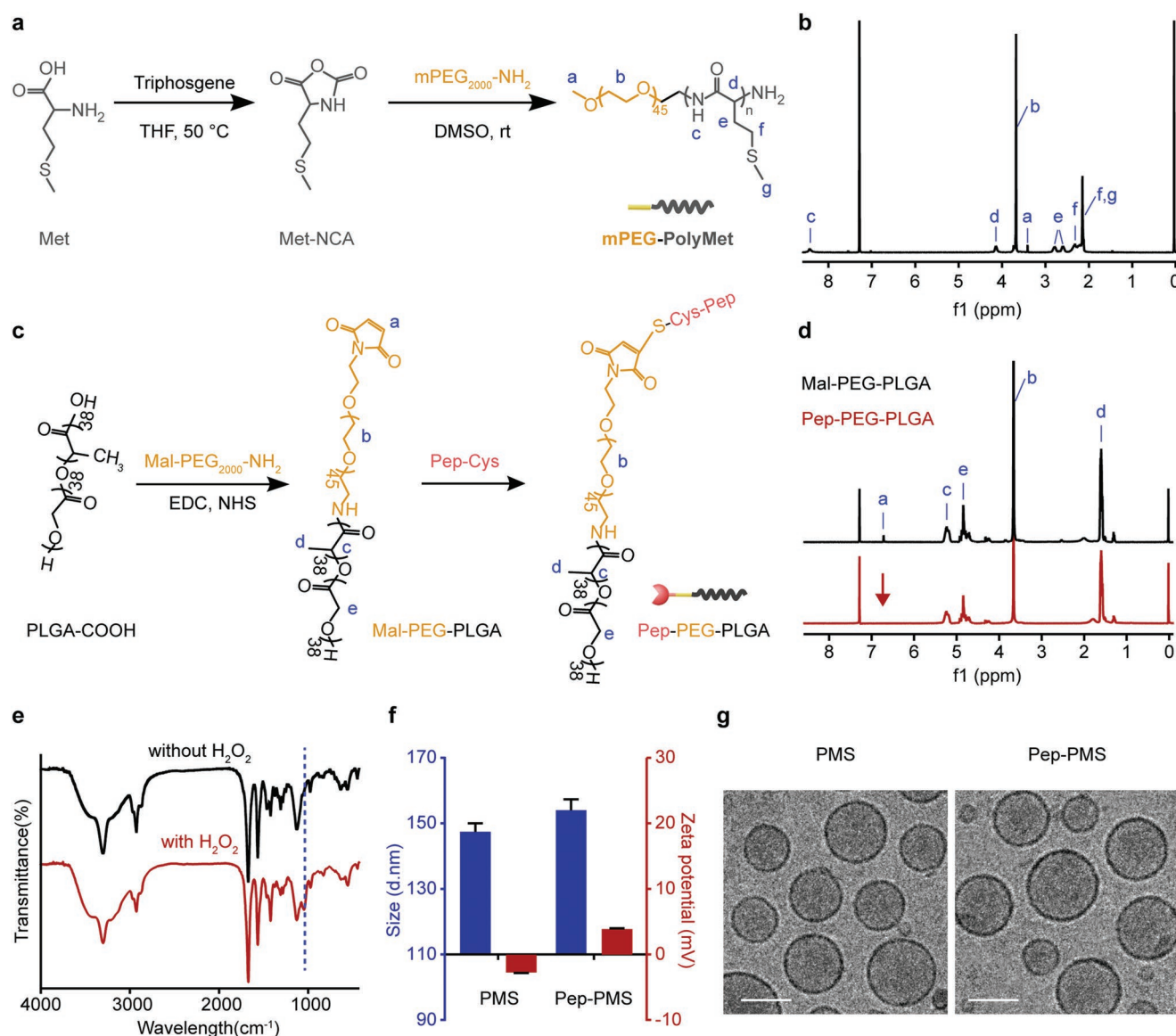
Figure 1. Preparation and characterization of functional polymers and PMS. a) The synthetic route to mPEG-PolyMet. b) ^{1}H NMR spectrum of mPEG-PolyMet. Peaks are assigned according to the labels in panel a. c) The synthetic route to Pep-PEG-PLGA. d) ^{1}H NMR spectra of Mal-PEG-PLGA and Pep-PEG-PLGA. Peaks are assigned according to the labels in panel (c). The red arrow indicates missing Mal group. e) FTIR spectrum of mPEG-PolyMet before and after incubation with H_2O_2. f) Size distribution and surface zeta potentials of PMS and Pep-PMS characterized by DLS. Data are means ± SD, $n = 3$. g) Cryo-TEM images of PMS and Pep-PMS. Scale bars: 100 nm.

the degree of polymerization of the Met block in mPEG-PolyMet was calculated to be 30 from the ^{1}H NMR spectrum and GPC result. Thus, the proportion of hydrophilic mass of the polymer was approximately 33.8%. As reported, polymers with a ratio of hydrophilic to total mass between 25% and 45% can generate PMS in water, so mPEG-PolyMet can theoretically form PMS in water and further respond to H_2O_2.[17]

2.1.2. Synthesis and Characterization of Pep-PEG-PLGA

To utilize the GM1-mediated transcytosis pathway, the GM1-targeting peptide (Pep) was conjugated to PEG-poly

(lactide-co-glycolide) and named Pep-PEG-PLGA (Figure 1c). Here, maleimide-polyethylene glycol amine (Mal-PEG$_{2000}$-NH$_2$) was first conjugated with PLGA-COOH through an amide reaction. Pep was then conjugated to Mal-PEG-PLGA to generate Pep-PEG-PLGA. The ^{1}H NMR peak corresponding to Mal groups at ≈6.7 ppm disappeared after Pep conjugation (Figure 1d), suggesting the successful synthesis of Pep-PEG-PLGA.

2.2. Preparation and Characterization of PMS

The ^{1}H NMR spectra of unmodified PMS prepared by the self-assembly of mPEG-PolyMet only showed peaks corresponding

to PEG, whereas those of PolyMet were missing (Figure S5, Supporting Information), confirming the formation of PMS. To prepare GM1-targeting PMS, a Pep-PEG-PLGA solution was premixed with an mPEG-PolyMet solution to obtain Pep-PMS. Dynamic light scattering (DLS) revealed that PMS were 147.4 nm in size with a zeta potential of −3.58 mV, whereas Pep-PMS were 154.0 nm in size with a zeta potential of +5.22 mV (Figure 1f). The particle size slightly increased and the zeta potential became weakly positive after Pep-PEG-PLGA was added, which further confirmed the surface modification of Pep. Then, the dispersibilities of PMS and Pep-PMS in different conditions such as culture medium and phosphate-buffered saline (PBS) were evaluated by recording the alteration of particle sizes and polydispersity indexes (PDIs). PMS and Pep-PMS showed outstanding dispersibilities under both conditions which may be caused by the existence of outer PEG corona after the formation of PMS (Figure S6, Supporting Information).[18] The morphologies of both types of PMS were observed by cryogenic transmission electron microscopy (cryo-TEM). Both PMS were spherical with cavities that were suitable for insulin encapsulation (Figure 1g). Additionally, the hydrophobic layer was clearly visualized. The entrapment efficiencies of insulin were determined to be 46.2% and 42.9%, and the loading capacities were 8.4% and 7.9% for PMS and Pep-PMS, respectively. The integrity of fluorescein isothiocyanate-labeled insulin (FITC-Ins)-loaded and 1,1′-dioctadecyl-3,3,3′,3′-tetramethylindocarbocyanine (DiI)-labeled Pep-PMS (double fluorophores-labeled Pep-PMS) was confirmed via fluorescence resonance energy transfer (FRET) measurements. Upon self-assembly into Pep-PMS, the emission intensity of FITC-Ins decreased at 520 nm and that of DiI increased at 575 nm owing to FRET in intact PMS (Figure S7, Supporting Information).

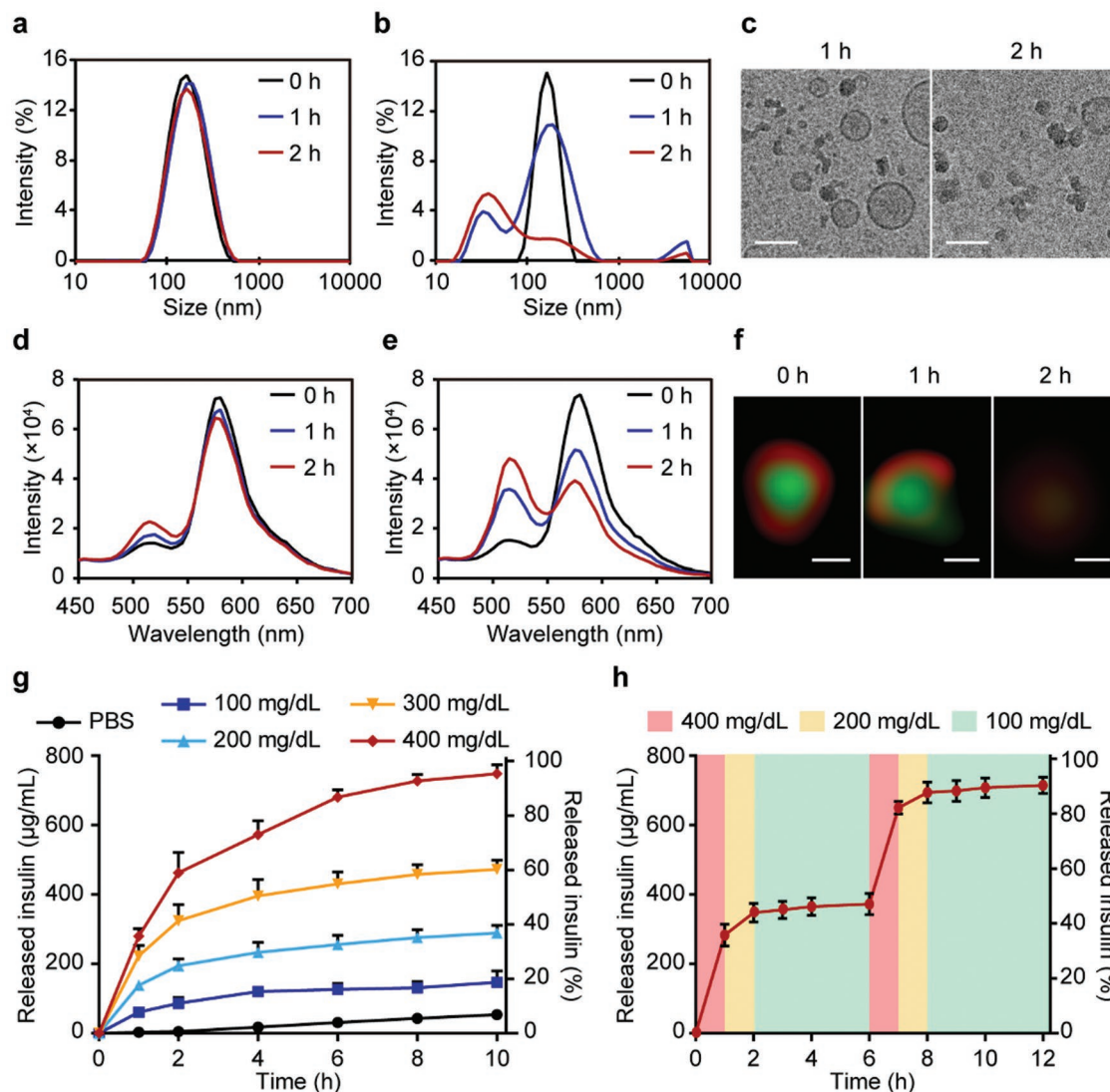### 2.3. Glucose-Responsive Insulin Release of Pep-PMS

To achieve the glucose-responsive insulin release properties, we followed a fact that sulfide groups can be oxidized to sulfoxides and ultimately to sulfones, turning hydrophobicity into hydrophilicity.[12c,16b,19] We first confirmed that H_2O_2 can be produced by coloaded GOx in the presence of glucose. It was obvious that the amount of H_2O_2 was positively related to glucose concentration (Figure S8, Supporting Information). The pH of the Pep-PMS solution significantly decreased after incubation with glucose (400 mg dL^{-1}), which demonstrated the successful diffusion of glucose into Pep-PMS, caused by the oxidation of glucose by the loaded GOx (Figure S9, Supporting Information). Afterward, the hydrophobic PolyMet groups would be oxidized by produced H_2O_2 leading to the dissolution of mPEG-PolyMet. Therefore, the H_2O_2-responsive dissociation of Pep-PMS was investigated. First, the absorbance of Pep-PMS significantly decreased over the course of 6 h, whereas it remained almost unchanged in the absence of the highest concentration of H_2O_2 (Figure S10a, Supporting Information). Moreover, the encapsulated insulin was released from Pep-PMS in PBS with H_2O_2 (Figure S10b, Supporting Information). These results demonstrated that Pep-PMS was H_2O_2 sensitive and could release insulin at different rates with respect to the glucose

concentration. It has been reported that a polymer contained thioether could remove the excess H_2O_2, the cellular toxicity could be lowered.[12c] This character is essential for nanocarriers to mimic endogenous insulin secretion because endogenous insulin is released quickly from pancreatic β cells only under hyperglycemic conditions.

The physicochemical changes of Pep-PMS, including the size and morphology, were observed in response to low and high glucose levels. The size of Pep-PMS remained almost unchanged under low glucose levels (**Figure 2**a). Under high glucose levels, however, the size decreased, and the size distribution became wider (Figure 2b). Cryo-TEM images showed that Pep-PMS were transformed into smaller PMS in 1 h, and most Pep-PMS were dissociated within 2 h (Figure 2c). Correspondingly, the FRET phenomenon changes further confirmed the dissociation degree of Pep-PMS at low and high glucose solutions. The fluorescence intensity of DiI slightly decreased and that of FITC-Ins slightly increased over 2 h in a low glucose solution (Figure 2d), from which we concluded that only a few Pep-PMS were dissociated. However, at high glucose concentrations, the fluorescence intensity of DiI significantly decreased and that of FITC-Ins remarkably increased in 2 h (Figure 2e). Stimulated emission depletion (STED) microscopy was used to visualize the morphological changes in double fluorophores-labeled Pep-PMS after incubating with a high glucose solution. At the start of the experiment (Figure 2f, 0 h), a DiI-labeled hydrophobic layer was observed encapsulating FITC-Ins. At 1 h, a gap, caused by the partial dissolution of mPEG-PolyMet, was clearly observed in the out layer, and FITC-Ins was released. Finally, at 2 h, both green and red fluorescence bands were barely observed which indicated that Pep-PMS was completely dissociated. In addition, confocal laser scanning microscopy (CLSM) was conducted to observe the release process of insulin from Pep-PMS. As shown in Figure S11 and Movies S1–S3 in the Supporting Information, the green fluorescence slightly decreased in a low glucose medium, whereas it rapidly decreased in a high glucose medium. These results implied that Pep-PMS could readily dissociate and release insulin rapidly under hyperglycemic conditions.

In vitro glucose-responsive insulin release profiles of Pep-PMS were studied by incubating Pep-PMS in PBS containing various concentrations of glucose (0, 100, 200, 300, and 400 mg dL^{-1}). Significantly faster insulin release was observed at hyperglycemic levels, whereas limited insulin release occurred at the normoglycemic (100 mg dL^{-1}) and control levels (PBS; Figure 2g). Moreover, if the glucose concentration changes with food intake, Pep-PMS could still release insulin at a corresponding rate (Figure 2h). Such a property would be beneficial to maintain euglycemia.

To evaluate the stability of PMS and Pep-PMS after oral delivery, NPs were incubated with PBS at different pH values mimicking gastrointestinal environments. As shown in Figure S12a in the Supporting Information, insignificant changes in size were observed after incubation with ultra acidic or nearly neutral conditions for 2 and 6 h, respectively. Furthermore, the insulin release profiles were recorded (Figure S12b, Supporting Information), and the results showed that all the insulin release rates were slow. The amount of insulin released from both PMS and Pep-PMS was less than

Figure 2. In vitro glucose-responsive insulin release of Pep-PMS. a) Size distribution of Pep-PMS after incubation with low glucose (100 mg dL^{-1}) solutions at 37 °C. b) Size distribution of Pep-PMS after incubation with high glucose (400 mg dL^{-1}) solutions at 37 °C. c) Cryo-TEM images of Pep-PMS after incubation with a high glucose solution at 37 °C for 1 and 2 h. Scale bars: 100 nm. d) Emission spectra of double fluorophores-labeled Pep-PMS with excitation at 420 nm after incubation with a low glucose solution at 37 °C for the indicated times. e) Emission spectra of double fluorophores-labeled Pep-PMS with excitation at 420 nm after incubation with high glucose solutions at 37 °C for the indicated times. f) In vitro glucose-responsive morphological change in single Pep-PMS in a high glucose solution observed by STED. Scale bars: 100 nm. g) In vitro insulin release profiles of Pep-PMS at different glucose concentrations at 37 °C. Data are means ± SD, $n = 3$. h) The insulin release profile of Pep-PMS at simulated diabetic blood glucose levels. Data are means ± SD, $n = 3$.

10% after incubation with ultra acidic conditions (pH 1.2) for 2 h and nearly neutral conditions (pH 6.8) for another 6 h. These results indicated that the PMS and Pep-PMS could keep stable in the gastrointestinal tract before being absorbed into systemic circulation.

An in vivo study through subcutaneous injection was performed in diabetic rats to evaluate the dynamic release of insulin from Pep-PMS. An oral glucose tolerance test (OGTT) was performed at 1 h after the subcutaneous injection of Pep-PMS. The blood glucose levels of diabetic rats treated with Pep-PMS increased relatively slowly after glucose administration and then declined to a normoglycemic state within

2 h, which was similar to the response observed in healthy rats (Figure S13a, Supporting Information). In contrast, blood glucose levels steadily increased in diabetic rats treated with insulin solution (Ins) during 2 h. To quantify the glucose response to the various formulations, the area under the curve (AUC) was calculated between 0 and 120 min for each group. As shown in Figure S13b in the Supporting Information, diabetic rats treated with Pep-PMS showed significantly improved blood glucose control to the glucose challenge compared with those treated with Ins. Importantly, when healthy rats were treated, the Ins group produced significantly reduced blood glucose levels compared to those produced by Pep-PMS

**ADVANCED
SCIENCE NEWS**

www.advancedsciencenews.com

**ADVANCED
FUNCTIONAL
MATERIALS**

www.afm-journal.de

(Figure S13c, Supporting Information), indicating that there was only little insulin leakage from Pep-PMS under normoglycemic conditions. Pep-PMS exhibited a remarkably lower hypoglycemia index compared to that exhibited by Ins (Figure S13d, Supporting Information).

2.4. Overcoming the Mucus Barrier

The mucus layer on the intestinal epithelial surface is considered a significant barrier to the absorption of nanocarriers.[20] Therefore, we examined the mucus penetration of PMS and Pep-PMS using mucus-secreting HT29-MTX-E12 cells. Both PMS could penetrate the mucus layer efficiently within 1 h (Figure S14, Supporting Information) likely because of their hydrophilic PEG surface and neutral charge. More Pep-PMS than PMS were internalized into the E12 cell monolayer, implying the significant influence of peptide modification.

2.5. GM1-Mediated Transcytosis of Pep-PMS

We studied whether Pep-PMS could traverse the intestinal epithelium by a mechanism similar to that used by the CTB, i.e., by GM1-mediated endocytosis, lysosome-evading pathway, Golgi-targeting pathway, and basolateral exocytosis (**Figure 3**a). Caco-2 cell monolayers were used to simulate the in vitro intestinal epithelium, and the cells were pre-incubated with GM1 (5×10^{-3} M) added to the cell medium for 4 h to increase cell-associated GM1 levels because of the negligible expression level of GM1 in the Caco-2 cells.[21] As shown in Figure S15 in the Supporting Information, after pre-incubation with GM1, Caco-2 cells expressed much more GM1 on the cytomembrane and the transcytosis of CTB and Pep across the Caco-2 cell monolayers was significantly enhanced. These results confirmed that abundant exogenous GM1 was successfully immobilized on the membranes of Caco-2 cells. Moreover, intestinal absorption of CTB was performed to illustrate the abundant existence of GM1 on the membrane. As shown in Figure S16 in the Supporting Information, the fluorescence intensity of Caco-2 with GM1 incubation was almost the same as that of the epithelium. It is reported that GM1 was expressed in the intestinal epithelium cells; thus, we can reasonably speculate that in vivo absorption pathways can be estimated from in vitro cellular results.[22]

After construction of the in vitro model, an MTT (3-(4,5-dimethylthiazol-2-yl)-2,5-diphenyltetrazolium bromide) assay was performed to evaluate the cytotoxicity of Pep-PMS. With concentrations ranging from 0.1 to 2 mg mL^{-1}, Pep-PMS did not significantly reduce cell viability (Figure S17a, Supporting Information). When encapsulated with GOx, no remarkable reduction in cell viability was observed as compared with that observed in the control groups, which may be caused by the ability of this type of polymer to remove excess H_2O_2 (Figure S17b, Supporting Information).[12c] The uptake of double fluorophores-labeled Pep-PMS by Caco-2 cells was then qualitatively studied using CLSM by comparing with double fluorophores-labeled PMS and FITC-Ins. The Pep-PMS group exhibited stronger green fluorescence intensity than the Ins- and PMS-treated groups (Figure 3b). Moreover, the green and

red fluorescence showed strong colocalization, indicating that both PMS and Pep-PMS remained intact in the Caco-2 cells. Insulin uptake by Caco-2 cells under different formulations was also quantitatively analyzed. The amount of insulin internalized into cells incubated with FITC-Ins-loaded Pep-PMS was 7.13- and 2.72-fold higher than that in cells treated with FITC-Ins and FITC-Ins-loaded PMS, respectively. Upon inhibition of GM1 with free Pep, the cellular uptake of insulin from Pep-PMS significantly decreased to levels similar to those from PMS. Similarly, cellular uptake of insulin from Pep-PMS was reduced in Caco-2 cells without GM1 (Figure 3c). These results demonstrated that cellular internalization of Pep-PMS mainly occurred through GM1-mediated active endocytosis.

In general, after being internalized into cells, nanocarriers may be transferred from endosomes to lysosomes for degradation.[23] Therefore, the fate of PMS and Pep-PMS in Caco-2 cells after endocytosis was studied. With GM1-targeting peptide modification, we proposed that the intracellular pathway could be the same as that of CTB, which is transported through the cell via GM1 binding. CTB is one of the subunits of cholera toxin (CT). When stably combined with GM1 existing in the cell membrane, CTB endocytosis could be mediated. Nest, the CTB-GM1 complex mainly traffics retrograde to the Golgi apparatus which may attribute to the lipid rafts at the cell surface. It is reported that such a retrograde pathway is not related to the lysosome.[9,24] As shown in Figure 3d, most green fluorescence of PMS was observed to colocalize with the red fluorescence of Lyso-Tracker Red-stained lysosomes at 1 and 2 h. However, few Pep-PMS were entrapped in the lysosomes. The colocalization coefficients of the Pep-PMS group were much lower than those of PMS group at 1 and 2 h (Figure 3e). From 3D images, we observed that Pep-PMS were close to the basolateral membrane, whereas lysosomes were present on the apical side (Figure S18, Supporting Information). Thus, Pep-PMS could avoid entering lysosomes. Furthermore, Pep-PMS were observed to largely colocalize with the Golgi apparatus at 1 and 2 h (Figure 3f). However, PMS could not be transferred to the Golgi apparatus. Correspondingly, the colocalization coefficients for the Pep-PMS group were much higher than those for PMS group at 1 and 2 h (Figure 3g). These results further confirmed that the GM1-mediated retrograde pathway had been successfully applied in Pep-PMS, which includes GM1-mediated lysosome-evading and Golgi-targeting intracellular pathway in Caco-2 cells. Such intracellular delivery of Pep-PMS may be beneficial to maintain the activity of encapsulated insulin.

Whether Pep-PMS could exit the cell monolayers by basolateral exocytosis was subsequently studied. After Caco-2 cell monolayers were incubated with double fluorophores-labeled Pep-PMS for 2 h, the basolateral medium was collected to detect the FRET signal of Pep-PMS. An intense FRET spectrum was observed (Figure 3h), which verified the transepithelial transport of intact Pep-PMS. Moreover, Pep-PMS were also visualized in the basolateral medium by cryo-TEM (Figure 3h, inset).

For the transepithelial pathway and efficiency of encapsulated insulin, the transepithelial electrical resistance (TEER) values were measured to monitor the integrity of tight junctions of Caco-2 cell monolayers. No significant decrease in TEER was observed after Caco-2 cell monolayers were incubated with any of the formulations (Figure S19, Supporting
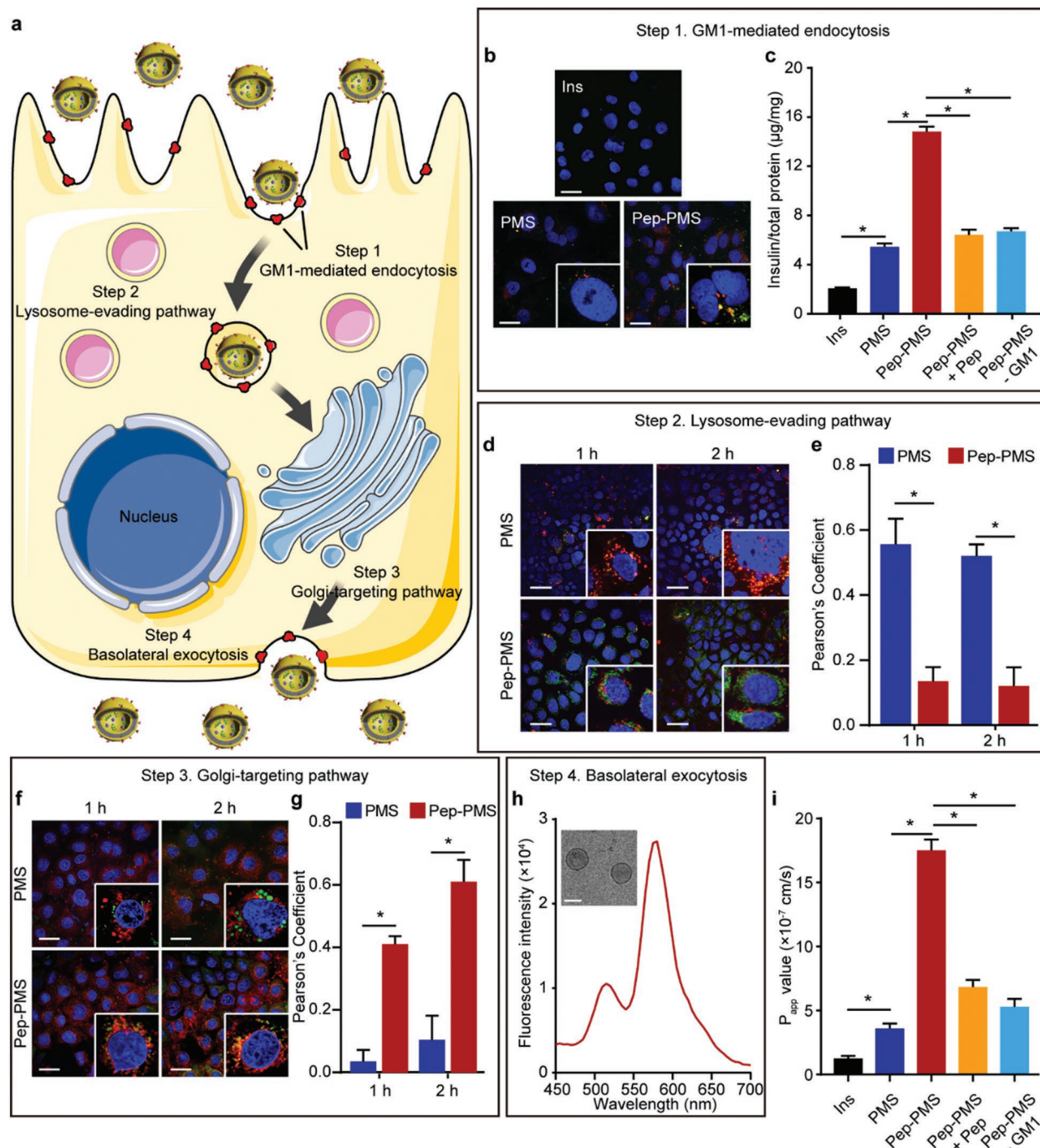
Figure 3. GM1-mediated transcytosis of Pep-PMS. a) Schematic illustration of the GM1-mediated transcytosis of Pep-PMS. b) CLSM images of Caco-2 cells incubated with FITC-labeled insulin (Ins), double fluorophore-labeled PMS, and double fluorophore-labeled Pep-PMS. Cell nuclei were stained with DAPI (blue). Scale bars: 20 μm. c) Quantitative determination of insulin cellular uptake for different treatments. "+ Pep" indicates that free peptide was added as an inhibitor. "- GM1" means that Caco-2 cells were not preincubated with GM1. Data are means ± SD, $n = 3$, p values were obtained using two-tailed Student's t test, *$p < 0.05$. d) CLSM images of the colocalization of FITC-Ins-loaded PMS and Pep-PMS (green) with lysosomes (red) after incubation for the indicated times. Enlarged images are shown in the white square. Cell nuclei were stained with Hoechst 33342 (blue). Scale bars: 20 μm. e) Pearson's coefficients of FITC-Ins-loaded PMS and Pep-PMS colocalized with lysosomes. Data are means ± SD, $n = 3$, p values were obtained using two-tailed Student's t test, *$p < 0.05$ as compared with PMS. f) CLSM images of the colocalization of PMS and Pep-PMS (green) with the Golgi apparatus (red) after incubation for the indicated times. Enlarged images are shown in the white square. Cell nuclei were stained with Hoechst 33342 (blue). Scale bars: 20 μm. g) Pearson's coefficient of PMS and Pep-PMS colocalized with the Golgi apparatus. Data are means ± SD, $n = 3$, p values were obtained using two-tailed Student's t test, *$p < 0.05$ as compared with PMS. h) Emission spectra and cryo-TEM images (inset) of the basolateral medium after the Caco-2 cell monolayer was incubated with double fluorophores-labeled Pep-PMS for 2 h. Scale bar: 100 nm. i) Apparent permeability coefficient (P_{app}) of insulin in different formulations across Caco-2 cell monolayers. Data are means ± SD, $n = 3$, p values were obtained using two-tailed Student's t test, *$p < 0.05$.

ADVANCED
SCIENCE NEWS
www.advancedsciencenews.com

ADVANCED
FUNCTIONAL
MATERIALS
www.afm-journal.de

Information), which confirmed the transcellular transport pathway of insulin. As shown in Figure 3i, the apparent permeability coefficient (P_{app}) of Pep-PMS was 17.52×10^{-7} cm s^{-1}, which was 14.02- and 4.85-fold higher than those of Ins and PMS, respectively. Moreover, after inhibition of GM1 with free Pep or in the Caco-2 cell monolayers without GM1, the P_{app} of insulin from Pep-PMS was significantly reduced, further indicating the important role of GM1 in the transcytosis of Pep-PMS. Overall, the results suggested that the use of Pep-PMS resulted in increased transepithelial transport of insulin via the GM1-mediated transcytosis pathway.

2.6. In Vivo Intestinal Absorption of Pep-PMS

To investigate the in vivo intestinal absorption of PMS, we visualized the transport of double fluorophores-labeled PMS and Pep-PMS in the intestinal villi by CLSM. Much more intense fluorescence was observed in the Pep-PMS-treated villi compared with that in the PMS group (**Figure 4**a). Moreover, almost all green fluorescence was colocalized with that of the red channel, indicating that both PMS and Pep-PMS remained intact. The results confirmed the better intestinal absorption of intact Pep-PMS versus PMS. The transepithelial transcytosis of Pep-PMS could lay the foundation of further studies on the in vivo distribution and glucose-responsive insulin release of Pep-PMS to intelligently control the blood glucose levels.

2.7. In Vivo Liver Accumulation of Pep-PMS

We investigated the glucose-responsive property and transcytosis character of Pep-PMS. The in vivo biodistribution of such PMS is vital to control blood glucose level. In a healthy body, endogenous insulin is secreted from β cells in the pancreas, after which it enters the liver through the portal vein and mainly accumulates there, resulting in a much higher concentration than that in the peripheral tissues. However, exogenous insulin goes into the peripheral tissues first and then moves to the liver, which is different from the pathway of endogenous insulin. To this end, first, we imaged the organs of rats 4 h after oral administration with FITC-Ins-loaded PMS and Pep-PMS using an in vivo imaging system (IVIS). Only the liver from rats treated with Pep-PMS yielded a strong FITC-Ins signal (Figure 4b). Correspondingly, the fluorescence intensity of Pep-PMS in the liver calculated from the homogenate was much higher than that of the other organs, which indicated Pep-PMS had mainly accumulated in the liver (Figure 4c).

To further assess the integrity of the PMS in the livers of healthy and diabetic rats, we labeled Pep-PMS using double fluorophores. We observed a strong fluorescence intensity corresponding to Pep-PMS in the liver lobules of healthy rats (Figure 4d), which confirmed the accumulation of Pep-PMS in the liver again. Moreover, green and red fluorescence colocalized well, indicating that Pep-PMS remained intact in the livers of healthy rats. In contrast, after administration to diabetic rats, Pep-PMS were found in lower abundance in the liver. This result might have arisen from the partial dissociation of Pep-PMS under hyperglycemic conditions.
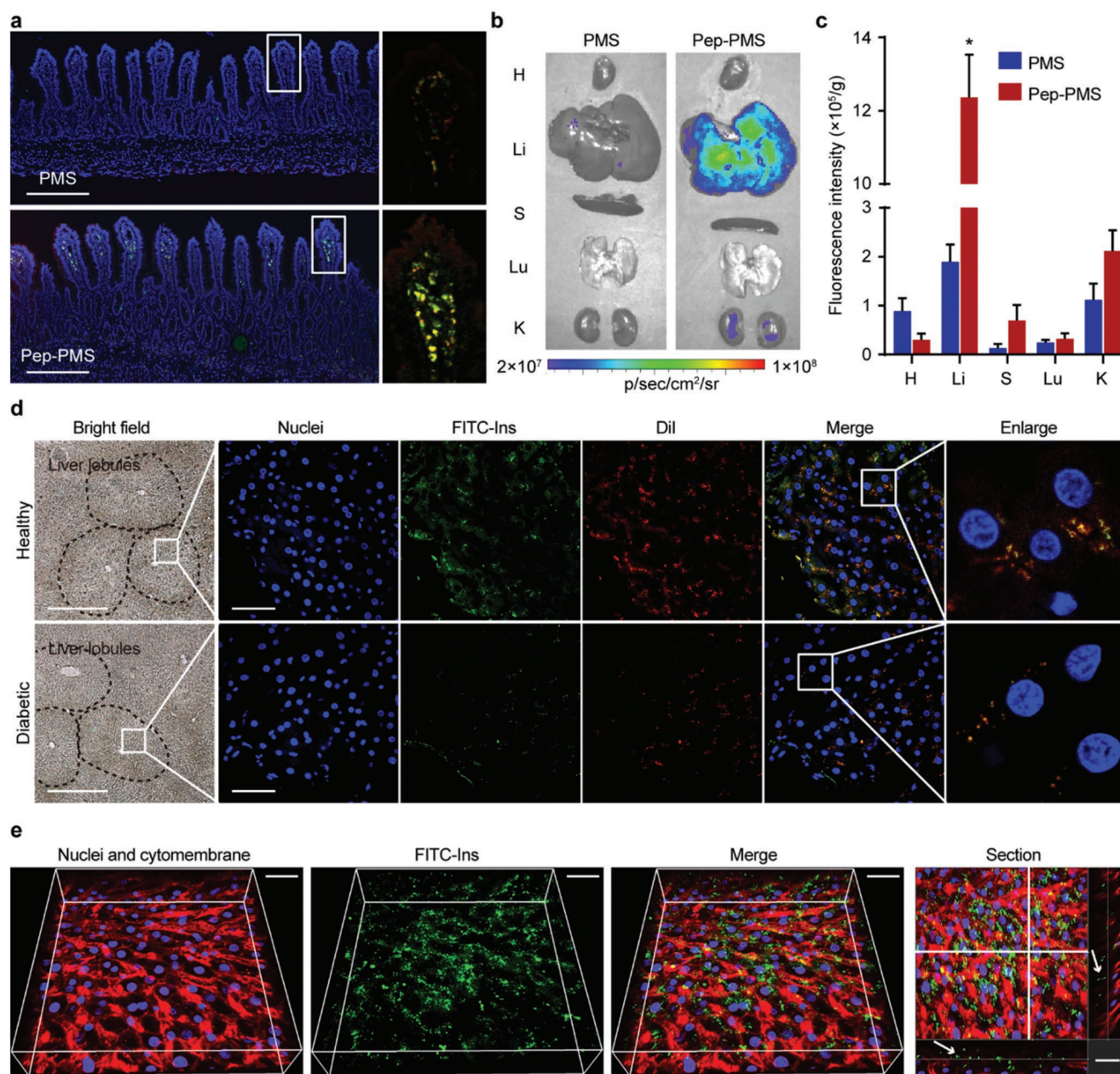
3D images of precision-cut liver slices obtained by CLSM were reconstructed to further examine the localization of Pep-PMS in the liver. Widespread green fluorescence of FITC-Ins-loaded Pep-PMS was observed in the liver slices (Figure 4e). Furthermore, from the xz and yz section images, we found that only a small number of Pep-PMS was internalized into the hepatocytes and that most Pep-PMS were localized in the space of Disse, where the blood flow rate becomes much slower and the fenestrations allow blood plasma to interact with hepatocytes.[25] Because insulin must interact with the insulin receptor in the cytomembrane of hepatocytes to elicit physiological effects, insulin released from Pep-PMS in the space of Disse under hyperglycemic conditions could directly bind to the insulin receptor on the hepatocytes. This might be attributed to the synergistic factors including size distribution, neutrally charged zeta potential, and PEG corona. Detailed mechanisms may require intense study in the future.

2.8. In Vivo Glucose-Responsive Insulin Release in the Liver

Delivering insulin carriers to the liver and releasing insulin in a glucose-responsive manner are both important to mimic endogenous insulin secretion. Here, to investigate glucose-responsive insulin release from Pep-PMS in the liver, precision-cut liver slices were separately incubated in PBS containing glucose at a low or high concentration. The intensity of the green fluorescence of FITC-Ins-loaded Pep-PMS changed slightly over 30 min in the low glucose (LG) group. However, in the high glucose (HG) group, we clearly observed that the green fluorescence significantly decreased in 30 min, indicating the accelerated dissociation of Pep-PMS (**Figure 5**a and Movies S4–S6, Supporting Information). Correspondingly, the relative integrated densities of Pep-PMS in the HG group at 15 and 30 min were markedly lower than those in the LG group (Figure 5b). These results demonstrated that Pep-PMS dissociated in the liver in response to elevated hepatic glucose concentrations.

The glucose-responsive dissociation of Pep-PMS in vivo in diabetic mice was confirmed using IVIS. A FRET pair, IR 783 and Tide Quencher 7WS (TQ7), was coloaded with insulin and GOx into Pep-PMS for in vivo imaging. According to the user manual, TQ7 can absorb the fluorescence of IR 783. Thus, the resulting Pep-PMS emitted weak fluorescence in vitro, as observed by the IVIS (Figure 5c). The diabetic mice were first injected subcutaneously with an insulin solution ($t = 0$ h) to lower the blood glucose level and avoid the release of Pep-PMS that was orally administrated following insulin injection. At 2 h post Pep-PMS administration, little fluorescence was detected in the mice and a glucose solution was administered to the mice through intraperitoneal injection to induce hyperglycemic conditions. At 3 h (1 h post-glucose administration), we observed an intense fluorescence signal in the liver (Figure 5c), which indicated that Pep-PMS dissociated and IR 783 was released in response to the elevated blood glucose level. Insulin would also be released which could result in a decrease in the blood glucose level. Consequently, the fluorescence intensity and thus Pep-PMS dissociation significantly decreased from 3 to 6 h. To simulate food intake-induced hyperglycemia, glucose was again administered at 6 h. As a

ADVANCED
SCIENCE NEWS
www.advancedsciencenews.com

ADVANCED
FUNCTIONAL
MATERIALS
www.afm-journal.de

Figure 4. In vivo intestinal absorption and liver accumulation of Pep-PMS. a) CLSM micrographs of small intestinal villi sections prepared from rat intestinal loops 2 h post administration with double fluorophore-labeled PMS or Pep-PMS. The boxed areas are enlarged at the right panel. Cell nuclei were stained with DAPI (blue). Scale bars: 200 μm. b) In vivo tissue distribution of FITC-Ins-loaded PMS and Pep-PMS after oral administration to healthy rats determined by IVIS. H, heart; Li, liver; S, spleen; Lu, lung; K, kidney. c) Quantitative determination of biodistribution of FITC-Ins-loaded PMS and Pep-PMS after oral administration to healthy rats. Fluorescence intensities of different tissue homogenates were measured. Data are means ± SD, $n = 3$, p values were obtained using two-tailed Student's t test, $*p < 0.05$, compared with fluorescence intensity in the livers of the PMS-treated rats. d) The accumulation of Pep-PMS in the liver after oral administration to healthy or diabetic rats. The black dashed circles indicate liver lobules. The boxed areas were observed at a higher magnification. Cell nuclei were stained with DAPI (blue). Scale bars in bright field images: 500 μm; CLSM images: 50 μm. e) 3D images showing the localization of FITC-Ins-loaded Pep-PMS in a precision-cut liver slice. Cell nuclei were stained with Hoechst 33342 (blue) and cytomembrane were stained with Alexa 555-wheat germ agglutinin (red). Scale bars: 30 μm.

result, a similar effect was observed. The fluorescence intensity in the liver increased at 7 h and then decreased from 7 to 10 h (Figure 5c). These results demonstrate that Pep-PMS can facilitate glucose-responsive insulin release in the liver. Thus, Pep-PMS could overcome multiple barriers including the mucus and intestinal epithelia after oral administration, and

importantly, intact Pep-PMS were found to accumulate abundantly in the liver and exhibit glucose-responsive behavior. By combining these series of phenomenon, we concluded that Pep-PMS could simulate the endogenous insulin secretion through oral administration, which may aid in better blood glucose control than other carriers.
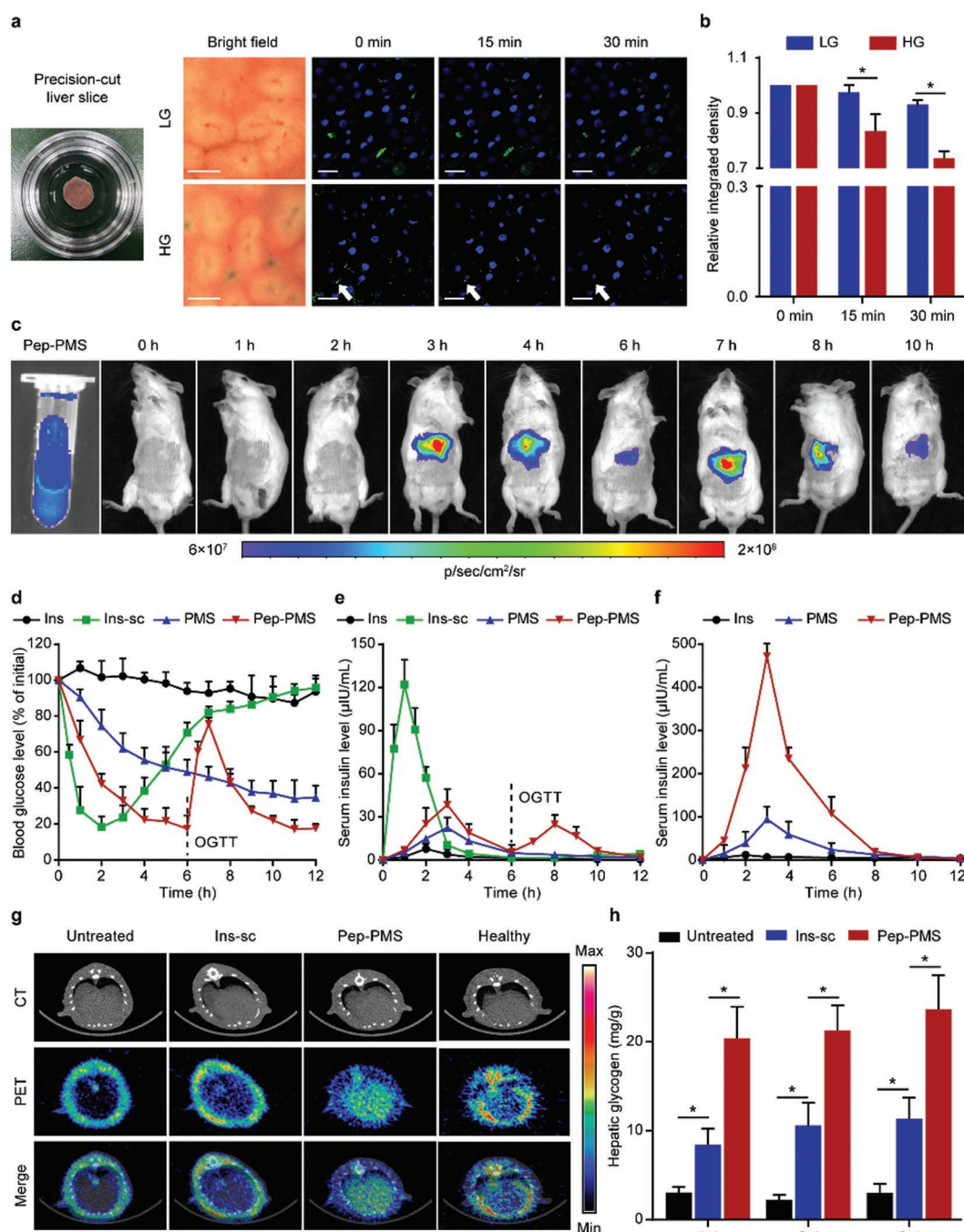
Figure 5. Hepatic glucose-responsive release, in vivo absorption of Pep-PMS and hepatic glucose utilization. a) Glucose-responsive release process of FITC-Ins-loaded Pep-PMS on precision-cut liver slices (shown in the picture on the left) from rats obtained 4 h after oral administration of Pep-PMS. LG, low glucose concentration (100 mg dL^{-1}). HG, high glucose concentration (400 mg dL^{-1}). Cell nuclei were stained with DAPI (blue). Scale bars in bright field images: 500 μm; CLSM images: 20 μm. b) Relative integrated densities of Pep-PMS measured by ImageJ in the precision-cut liver slices. Data are means ± SD, $n = 3$, p values were obtained using two-tailed Student's t test, $*p < 0.05$ as compared with LG. c) Live animal imaging to examine the glucose-responsive dissociation of Pep-PMS in a diabetic mouse. IR 783, TQ7, insulin, and GOx were coloaded into Pep-PMS. Pep-PMS were orally administered to the diabetic mouse following insulin injection at 0 h. A glucose solution was administered via intraperitoneal injection at a dose of 1.5 g kg^{-1} at 2 and 6 h. d) Blood glucose level versus time profiles of diabetic rats following oral gavage of Ins, insulin-loaded PMS, and Pep-PMS (100 IU kg^{-1}) and subcutaneous injection of insulin solution (Ins-sc, 5 IU kg^{-1}). A glucose solution (2 g kg^{-1}) was orally administered to the diabetic rats 6 h after oral gavage of insulin-loaded Pep-PMS to simulate food intake. Data are means ± SD, $n = 6$. e) Peripheral serum insulin level versus time profiles of diabetic rats following oral gavage of Ins, insulin-loaded PMS, and Pep-PMS (100 IU kg^{-1}) and subcutaneous injection of insulin solution (5 IU kg^{-1}). Data are means ± SD, $n = 6$. f) Portal serum insulin level versus time profiles of diabetic rats following oral gavage of Ins, insulin-loaded PMS, and Pep-PMS (100 IU kg^{-1}). g) PET/CT images of ^{18}F-FDG uptake in the liver of the diabetic rats administered with different formulations and healthy rat. h) Hepatic glycogen content of the diabetic rats treated with different insulin formulations for several days. Data are means ± SD, $n = 6$, p values were obtained using two-tailed Student's t test, $*p < 0.05$.

2.9. In Vivo PD and Pharmacokinetics (PK) Studies

The hypoglycemic effect and PK of Pep-PMS in diabetic rats were studied. As anticipated, oral administration of Ins (100 IU kg^{-1}) failed to decrease the blood glucose level, indicating poor oral absorption of free-form insulin (Figure 5d). Subcutaneous injection of insulin (5 IU kg^{-1}) produced a sharp decrease in the blood glucose level, which reached a minimum at 2 h post insulin injection and gradually returned to baseline. In contrast, oral gavage of insulin-loaded PMS (100 IU kg^{-1}) induced a slower but prolonged hypoglycemic effect for up to 12 h. The blood glucose level of diabetic rats administered the insulin-loaded Pep-PMS (100 IU kg^{-1}) was rapidly reduced, and a normal glucose level was attained within 6 h. To simulate food intake, an OGTT was performed at 6 h after gavage of Pep-PMS. The blood glucose level increased 1 h post glucose administration and then decreased to normoglycemia again. No hypoglycemic phenomenon occurred in these diabetic rats treated with Pep-PMS. The results demonstrated that a high dose of Pep-PMS can respond to hyperglycemia and release insulin twice to maintain blood glucose levels.

Consistent with the PD results, the PK profiles (Figure 5e) showed that the Ins-sc group exhibited a sharp increase in peripheral serum insulin levels 1 h post injection, and the levels rapidly decreased again in the following 2–3 h. In contrast, oral administration of insulin-loaded PMS and Pep-PMS led to a slower increase in peripheral serum insulin levels, and the maximum insulin concentrations appeared at 3 h post PMS administration. Higher peripheral serum insulin levels were obtained in the Pep-PMS group than in the Ins and PMS groups. Additionally, after OGTT was performed in the Pep-PMS group, one more insulin peak was observed, which demonstrated insulin release in response to the elevated glucose level. As shown in **Table 1**, the AUC of serum insulin level in the Pep-PMS was 172.8 μIU*h mL^{-1}, with a relative bioavailability of 3.9%. Because Pep-PMS largely accumulated in the liver, there might be a bias in using the peripheral serum insulin concentration to calculate the relative bioavailability. Thus, portal blood samples of diabetic rats treated with Ins, insulin-loaded PMS, and insulin-loaded Pep-PMS were collected to measure the portal serum insulin concentration. The absorption of Pep-PMS into the portal blood was significantly higher than that of PMS and Ins during 1–6 h post-administration (Figure 5f). Compared with that of the Ins group, the total insulin absorptions from PMS and Pep-PMS were 4.9- and

Table 1. Pharmacokinetic parameters calculated from peripheral serum insulin versus time profiles of different insulin formulations following administration to diabetic rats.

	Ins-sc	Ins	PMS	Pep-PMS
Dose (IU kg^{-1})	5	100	100	100
AUC (μIU*h mL^{-1})	221.7 ± 11.3	22.5 ± 5.4	85.0 ± 7.0	172.8 ± 15.8
C_{max} (μIU mL^{-1})[a]	121.9 ± 17.2	7.6 ± 3.3	22.5 ± 7.2	38.4 ± 11.0
T_{max} (h)[b]	1	2	3	3
F (%)[c]	100	0.5	1.9	3.9

[a]C_{max}: maximum serum insulin concentration; [b]T_{max}: time at C_{max}; [c]F: relative bioavailability.

Table 2. Analysis of portal serum insulin versus time profiles of different insulin formulations following administration to diabetic rats.

	Ins	PMS	Pep-PMS
Dose (IU kg^{-1})	100	100	100
AUC (μIU*h mL^{-1})	66.4 ± 11.8	326.7 ± 55.1	1346.0 ± 95.8
Ratio[a]	–	4.9	20.3

[a]Ratio: increased AUC ratio of PMS and Pep-PMS compared to the Ins group.

20.3-fold higher, respectively (**Table 2**). We can reasonably speculate that the improved oral delivery efficiency of insulin was caused by the reasonable design of Pep-PMS. Such insulin carriers could utilize the GM1-mediated transcytosis to overcome multiple barriers and then simulate the endogenous insulin secretion in liver. They can avoid the complication of hyperinsulinemia and prevent the wastage of insulin, thus helping control blood glucose more strictly.

2.10. In Vivo Hepatic Glucose Utilization Studies

By now, most studies have been focusing on lowering the blood glucose levels alone while neglecting the glucose metabolism and utilization conditions. Actually, under physiological conditions, food intake shifts hepatic glucose metabolism from glucose production to glucose storage; insulin is a crucial regulator of this transition, and it primarily acts by activating glycogen synthase.[26] This process is crucial to blood glucose homeostasis because glycaemia is maintained by degradation of hepatic glycogen during a fasting state. As reported, even optimized systemic insulin substitution cannot resolve the defect in postprandial liver glycogen storage in type I diabetic patients.[5] Here, we further investigated the hepatic glucose utilization induced by Pep-PMS in diabetic rats, including hepatic glucose uptake and hepatic glycogen production. As shown in Figure 5g, [18F]-fluorodeoxyglucose (^{18}F-FDG) was barely transported into the liver of untreated diabetic rats because little insulin was produced. After treating the diabetic rat with a subcutaneous injection of insulin, a small part of insulin entered the liver via systemic circulation. Thus, a higher ^{18}F-FDG uptake was observed in the liver of the diabetic rat. Compared with the untreated and Ins-sc groups, Pep-PMS induced the highest ^{18}F-FDG uptake in the liver, similar to the level of ^{18}F-FDG in the liver of healthy rats, which could be attributed to the accumulation of Pep-PMS in the liver followed by the release of insulin under hyperglycemic condition. The quantitative analysis of SUV-bw values in the liver from different groups further confirmed the advantages of Pep-PMS (Figure S20, Supporting Information).

It is reported that insulin acts on liver insulin receptors to directly activate glycogen synthesis.[3] We further measured the hepatic glycogen contents of diabetic rats treated with different formulations. After treating for 1, 2, and 3 days, the subcutaneous injection of insulin could lead to a higher hepatic glycogen content compared with the untreated diabetic rats. This content was however still less than that in diabetic rats treated with Pep-PMS (Figure 5h). The higher glycogen production of Pep-PMS-treated rats is ascribed to the higher glucose uptake in the liver. When treating for 7 days, the production

level of glycogen in Pep-PMS-treated rats still remained the highest as compared with other groups (Figure S21a, Supporting Information). Meanwhile, the body weight changes of rats were recorded, and no dramatic decrease appeared in Pep-PMS treated groups, which indicated the in vivo safety of Pep-PMS (Figure S21b, Supporting Information). Therefore, orally delivered Pep-PMS can improve the hepatic glucose utilization of diabetic rats by inducing enough glucose transformed into hepatic glycogen to ensure the blood glucose homeostasis between meals.

Here, we further tested the biodegradability and biocompatibility of PMS to verify the promising application for oral delivery by using GPC, mass spectrometry (MS), and hematoxylin and eosin (HE) staining.[27] After incubation with PBS for 3 days, the GPC and MS results showed that some of the polymers were degraded into nontoxic small molecules which may be PEG and methionine according to the molecular weight observed via MS (Figure S22, Supporting Information). To investigate the biocompatibility of Pep-PMS, histological images of the liver and intestine obtained using HE staining were collected after 1 week of administration once a day. The amount of polymer used here (912 mg kg^{-1}) was 20 times higher than those in the effective dose (45.6 mg kg^{-1}). As shown in Figure S23 in the Supporting Information, compared with the PBS-treated diabetic rat, no toxic signals in the liver or intestine were observed. After that, we further tested the biocompatibility of Pep-PMS containing GOx. No significant tissue damage was observed after oral administration for 14 days (Figure S24, Supporting Information). The amount of polymer used here was the same as those in the effective dose (45.6 mg kg^{-1}). Meanwhile, the blood biochemical indexes, particularly the aspartate aminotransferase and alkaline phosphate, were measured at the end of this experiment. It showed insignificant changes for Pep-PMS containing GOx-treated groups which indicated that Pep-PMS containing GOx had less liver toxicity (Figure S25, Supporting Information). As reported before, the polymer composed by PEG and poly(amino acids) has excellent biodegradability and biocompatibility, which was further confirmed by our result.[12c,15] Thus, all these results indicated that our rationally designed Pep-PMS had favorable biodegradability and biocompatibility with the liver and intestine, and delivery through oral administration was found to be suitable.

3. Conclusion

In summary, we have designed a novel oral insulin delivery system, GM1-targeting PMS (Pep-PMS), which was self-assembled by an amphiphilic diblock polymer (mPEG-PolyMet), to traverse the intestinal epithelium and accumulate in the liver. Pep-PMS can serve as a reservoir and further exhibit insulin secretion in a glucose-responsive manner in response to hyperglycemia, thus effectively controlling the postprandial blood glucose and improving the hepatic glucose utilization. Notably, the biomimetic strategy proposed here could be widely applicable for all insulin delivery systems regardless of the administration route. This may open up new avenues of investigations and potential uses of smart insulin carriers for the management of diabetes mellitus.

4. Experimental Section

Experimental Reagents: L-Methionine (Met), triphosgene, anhydrous tetrahydrofuran (THF), and anhydrous dimethyl sulfoxide (DMSO) were purchased from Sinopharm Chemical Reagent Co., Ltd. (Shanghai, China). Methoxypolyethylene glycol amine (mPEG$_{2000}$-NH$_2$) and maleimide-polyethylene glycol amine (Mal-PEG$_{2000}$-NH$_2$) were purchased from Shanghai ToYongBio Tech. Inc. (Shanghai, China). Poly (D, L-lactic-co-glycolic acid) (PLGA-COOH, MW: 5,000) was purchased from Ruixi Biological Technology Co., Ltd. (Xi'an, China). The GM1-targeting peptide (Pep) GWWYKGRARPVSAVAC was purchased from Bankpeptide Biological Technology Co., Ltd. (Hefei, China). Human insulin was provided as a gift by Novo Nordisk A/S. Glucose oxidase (GOx) was obtained from Meilun Biotech Co., Ltd. (Dalian, China). GM1 was purchased from Yuancheng Gongchuang Technology Co., Ltd. (Wuhan, China). Alexa 555-labeled wheat germ agglutinin (Alexa 555-WGA) was purchased from Thermo Fisher Scientific (Oregon, USA). Lyso-Tracker Red, Golgi-Tracker Red, DAPI (4′,6-diamidino-2-phenylindole), and Hoechst 33342 were purchased from Beyotime Biotechnology Co., Ltd. (Shanghai, China). IR 783 was purchased from Sigma-Aldrich (Shanghai, China). TQ7 was purchased from AAT Bioquest (California, USA). Human insulin ELISA kits were purchased from Mercodia (Uppsala, Sweden). Glycogen ELISA kits were purchased from Solarbio Science and Technology Co., Ltd. (Beijing, China). All other reagents were purchased from Sinopharm Chemical Reagent Co., Ltd. (Shanghai, China).

Synthesis of Met-NCA: The monomer Met-NCA was synthesized from Met as reported with a slight modification.[15a,28] In brief, Met (2 g, 13.4 mmol) was suspended in anhydrous THF (80 mL). Then, triphosgene (2 g, 6.7 mmol) was added. The reaction mixture was stirred at 50 °C for 2 h. After the suspension cleared, the reaction mixture was concentrated under reduced pressure using a rotary evaporator. The product was finally purified by silica gel chromatography using EtOAc/ petroleum ether (3:7 then 1:1, v/v) as the eluent. After removing the solvents by using a rotary evaporator, a small amount of the pure product was dissolved in CDCl$_3$ and characterized by NMR spectroscopy (Avance III 400, Bruker, Switzerland).

Synthesis and Characterization of mPEG-PolyMet: mPEG$_{2000}$-NH$_2$ (0.8 g, 0.4 mmol) was dissolved in anhydrous DMSO (60 mL). A solution of Met-NCA (3.5 g, 20 mmol) in anhydrous DMSO (5 mL) was then quickly added to the reaction with stirring. The polymerization was carried out under vacuum at room temperature for 48 h. The product was precipitated from the reaction mixture by adding diethyl ether (600 mL). The precipitate was collected by centrifugation (10 000 g, 10 min) and washed with diethyl ether and water five times. The polymer was dried in a vacuum oven under room temperature, and a small amount was dissolved in CDCl$_3$ and characterized by NMR spectroscopy. GPC was performed on Tosoh HLC-8320 with RI detector. The separation of mPEG-PolyMet was achieved on TSKgel SuperMultiporeHZ-M column (Tosoh, 4 μm, 4.6 mm × 150 mm) at 50 °C using THF as mobile phase. The molecular weight of polymers was calibrated against standard PstQuick MP-M (0.3–700 kDa).

To confirm the H$_2$O$_2$-sensitive property of mPEG-PolyMet, the polymer was incubated with certain H$_2$O$_2$ (200 × 10^{-6} M) for 4 h, the structural changes of this polymer was investigated using FTIR (Thermo Fisher IS5, USA) after dialysis overnight.

Synthesis of Pep-PEG-PLGA: First, Mal-PEG-PLGA was synthesized by conjugating Mal-PEG$_{2000}$-NH$_2$ with PLGA-COOH through a coupling reaction. Then, Pep-PEG-PLGA was synthesized by conjugating the maleimide groups of PEG-PLGA with the thiol groups of Pep according to a previous report.[29] Generally, PLGA-COOH (0.2 g, 40 μmol) was dissolved in DMF (5 mL), and excess ethyl(dimethylaminopropyl) carbodiimide (23 mg, 120 μmol) and N-hydroxysuccinimide (9.2 mg, 80 μmol) were added. Then, Mal-PEG$_{2000}$-NH$_2$ (80 mg, 40 μmol) was added and allowed to react for 24 h, followed by dialysis (MW cutoff: 3500 Da) against water for 24 h. The product was lyophilized, and a small amount was dissolved in CDCl$_3$ and characterized by NMR spectroscopy. Next, Mal-PEG-PLGA was conjugated with Pep (72.3 mg,

40 µmol) in DMF (5 mL) for 24 h at room temperature. Finally, the reaction solution was dialyzed (MW cutoff: 3500 Da) against water for 24 h and then freeze-dried to obtain the Pep-PEG-PLGA polymer. A small amount of the polymer was dissolved in CDCl$_3$ and characterized by NMR spectroscopy.

Preparation and Characterization of PMS: Pep-PMS were prepared by the solvent evaporation method.[12b] In brief, mPEG-PolyMet (40 mg) and Pep-PEG-PLGA (10 mg) were dissolved in THF (5 mL), followed by injection of aqueous solution (10 mL) with or without human insulin (10 mg) and GOx (1 mg). The mixture was stirred at room temperature for 30 min, and then THF was removed by bubbling with N$_2$. The unloaded insulin was removed by gel filtration through Sephadex G50. For the preparation of PMS, 10 mg of Pep-PEG-PLGA was replaced by 10 mg of mPEG-PolyMet, and a similar procedure was used. Both PMS were stored at 4 °C for further studies. To prepare double fluorophores-labeled PMS and Pep-PMS, DiI in ethanol (1 mg mL^{-1}, 100 µL) was added into the polymer solution (50 mg), FITC-Ins (10 mg) and GOx were loaded into PMS and Pep-PMS. After gel filtration, the FRET was detected with excitation at 420 nm by a microplate reader.

The mean particle size, PDI, and zeta potential of PMS and Pep-PMS were measured using a Malvern Zetasizer NanoZS (Malvern Instruments, UK). The entrapment efficiency (EE) and loading capacity (LC) were determined after centrifugation of PMS (18 000 g, 30 min) at 4 °C, and the amount of insulin in the supernatant was quantified using high performance liquid chromatography (HPLC; Agilent 1200, USA). The morphology of PMS and Pep-PMS was observed by cryo-TEM (TF20, FEI, USA).

In Vitro Glucose-Responsive Insulin Release Studies: Pep-PMS (10 mg) were incubated in PBS (1 mL) containing glucose (100 and 400 mg dL^{-1}) for 2 h at 37 °C. The particle sizes were measured by DLS at different time points. In addition, the morphology of Pep-PMS in the high glucose solution (400 mg dL^{-1}) was observed by cryo-TEM. Double fluorophores-labeled Pep-PMS (10 mg) were incubated in PBS (1 mL) containing glucose (100 and 400 mg dL^{-1}) at 37 °C. At predetermined time points, the FRET emission of the samples was measured with excitation at 420 nm by a microplate reader. At 0, 1, and 2 h after incubation, samples from the high glucose solution were withdrawn for STED observation (TCS SP8, Leica, Germany).

In addition, insulin and GOx-loaded Pep-PMS (10 mg) were added to PBS (1 mL) containing glucose (0, 100, 200, 300, and 400 mg dL^{-1}). The suspensions were incubated at 37 °C on a shaker at 100 rpm. At predetermined time points, samples (50 µL) were removed for analysis and replaced with fresh medium (50 µL). The insulin concentrations in the withdrawn samples were determined by HPLC after centrifugation (18 000 g, 30 min) at 4 °C. Furthermore, we studied the insulin release of Pep-PMS in repeated cycles with high, medium, and low glucose concentrations. In brief, insulin and GOx-loaded Pep-PMS (10 mg) were added to PBS (1 mL) containing glucose (400 mg dL^{-1}) and incubated for 1 h at 37 °C. After collection by centrifugation (18 000 g, 30 min) at 4 °C, Pep-PMS were incubated in PBS (1 mL) containing glucose (200 mg dL^{-1}) for 1 h at 37 °C. Pep-PMS were then collected and transferred to PBS (1 mL) containing glucose (100 mg dL^{-1}) and incubated for 4 h at 37 °C. Then, the particles were collected as before and subjected to a second cycle, as described above. At predetermined time points, the samples (50 µL) were taken out for analysis and replaced by fresh medium (50 µL). The insulin concentrations in the withdrawn samples were determined by HPLC after centrifugation (18 000 g, 30 min) at 4 °C.

Cellular Uptake Studies: Caco-2 cells were cultured on glass coverslips in a 12-well plate for 3 days. Before experiments, the cells were incubated with GM1 (5×10^{-3} M) added to the cell medium for 4 h. Then, the cells were washed twice with PBS and equilibrated with prewarmed PBS for 30 min at 37 °C in a 5% CO$_2$ incubator. To visualize the uptake and integrity of PMS, Caco-2 cells were incubated with either FITC-Ins solution, double fluorophores-labeled PMS, or double fluorophores-labeled Pep-PMS at an FITC-Ins concentration of 50 µg mL^{-1} for 2 h at 37 °C. The cells were then washed with PBS and fixed with 4% paraformaldehyde. After staining with DAPI for 10 min,

the slides were washed and observed by CLSM (FV1000, Olympus, Japan). To quantitatively measure the uptake and further evaluate the role of GM1 in the uptake of Pep-PMS, Caco-2 cells were incubated for 2 h with either FITC-Ins solution, FITC-Ins-loaded PMS, FITC-Ins-loaded Pep-PMS, or FITC-Ins-loaded Pep-PMS with free Pep (100 × 10^{-6} M) at an FITC-Ins concentration of 50 µg mL^{-1}. In addition, the cellular uptake of Pep-PMS was studied in Caco-2 cells without prior incubation with GM1. After incubation with different formulations for 2 h at 37 °C, the cells were washed with PBS and lysed in RIPA lysis buffer. The amounts of FITC-Ins and total protein were determined using a microplate reader and BCA protein assay kit, respectively.

Intracellular Fate of PMS: The intracellular fate of PMS and Pep-PMS was observed by colocalization with lysosomes and the Golgi apparatus. In brief, Caco-2 cells were first stained with Hoechst 33342 and Lyso-Tracker Red or Golgi-Tracker Red for 30 min. Subsequently, FITC-Ins-loaded PMS or FITC-Ins-loaded Pep-PMS at an FITC-Ins concentration of 50 µg mL^{-1} were added to the cells, which were then incubated at 37 °C in a 5% CO$_2$ incubator. After 1 and 2 h, the cells were observed by CLSM. Pearson's coefficients of PMS and Pep-PMS were quantified using ImageJ software (NIH, USA).

Insulin Transepithelial Transport Studies: Transwell inserts with TEER values in the range of 1000–1200 Ω × cm^2 were used for the following experiments. Caco-2 cell monolayers were washed twice with PBS and incubated with prewarmed PBS for 30 min at 37 °C in a 5% CO$_2$ incubator. The donor solutions were prepared by diluting an aliquot of FITC-Ins, FITC-Ins-loaded PMS, or FITC-Ins-loaded Pep-PMS solution into PBS to yield a final insulin concentration of 50 µg mL^{-1}. Moreover, Caco-2 cell monolayers with free Pep (100 × 10^{-6} M) or without prior GM1 incubation were used to evaluate the role of GM1 on the transport of Pep-PMS. At different time intervals, 200 µL of each acceptor sample was removed, and replaced by the same volume of fresh PBS. TEER values were also measured to determine the integrity of tight junctions. The amounts of FITC-Ins were measured using a microplate reader. The P_{app} values of insulin from the different treatments were calculated as reported.[30]

Caco-2 cell monolayers were also incubated with double fluorophores-labeled Pep-PMS. After 2 h, the basolateral medium was collected and concentrated by ultrafiltration (MW cutoff: 100 kDa). Subsequently, FRET emission was measured on a microplate reader with excitation at 420 nm. In addition, the presence of intact Pep-PMS in the basolateral medium was verified by cryo-TEM.

Animal Models: Male Sprague–Dawley rats (180–200 g) and ICR mice (18–20 g) were provided by the Animal Experiment Center of Shanghai Institute of Materia Medica, China. All of the animal experiments were performed in compliance with the Institutional Animal Care and Use Committee (IACUC) guidelines of Shanghai Institute of Materia Medica. For induction of type I diabetes, the rats were injected with streptozotocin (65 mg kg^{-1}) dissolved in a citrate buffer (10 × 10^{-3} M, pH 4.5), and the mice were injected at a dose of 150 mg kg^{-1} as previously described.[31] A glucose meter (On Call EZ, Acon Biotechnology, Hangzhou, China) was used to determine blood glucose levels. Rats and mice were regarded as diabetic if their fasting blood glucose levels were higher than 300 mg dL^{-1} 1 week after injection.[32]

Absorption Studies on Intestinal Loop: The intestinal absorption of PMS and Pep-PMS was assessed using the ligated intestinal loop model. In brief, after a rat was anesthetized, the abdomen was exposed, and then, 5 cm loops of small intestine were made by ligation at both ends. Next, 0.4 mL of double fluorophores-labeled PMS or Pep-PMS was injected into the loops. After 2 h, the rat was sacrificed, and both loops were excised and washed with PBS. Subsequently, the loops were fixed with 4% paraformaldehyde at 4 °C for 2 h. 20 µm sections of each loop were cut using a cryostat (Leica CM 1950) and then stained with DAPI for 10 min. The tissues were observed by CLSM.

In Vivo Biodistribution Studies: Healthy rats were fasted overnight before oral gavage of FITC-Ins-loaded PMS and Pep-PMS (10 mg). After 4 h, the rats were sacrificed, and the heart, liver, spleen, lung, and kidney were harvested. First, ex vivo fluorescent images of the organs were obtained using the IVIS Spectrum system (Perkin Elmer, USA). Then,

0.5 g of each organ was homogenized in PBS containing 50% RIPA lysis buffer (2 mL). The lysate of each organ was centrifuged at 6000 g at 4 °C for 20 min, and then the fluorescence intensity of the supernatant was measured using a microplate reader.

Liver Accumulation Studies: Healthy and diabetic rats were fasted overnight before oral gavage with double fluorophores-labeled Pep-PMS (10 mg). After 4 h, the rats were sacrificed, and the livers were harvested. After washing with PBS, the livers were fixed with 4% paraformaldehyde at 4 °C for 2 h. 20 μm sections of the livers were cut using a cryostat (Leica CM 1950) and then stained with DAPI for 10 min. The tissues were observed by CLSM.

Localization and Glucose-Responsive Release Studies of Pep-PMS on Precision-Cut Liver Slices: One healthy rat was fasted overnight before oral gavage of FITC-Ins loaded Pep-PMS (10 mg). After 4 h, the rat was sacrificed, and the liver was harvested. Precision-cut liver slices were obtained according to the reported literature.[33] Some liver slices were stained with Hoechst 33342 and Alexa 555-WGA for 15 min. Z-stack images were captured using CLSM and processed with the 3D reconstruction software Imaris (Bitplane AG, Switzerland).

On the other hand, after staining with Hoechst 33342 for 15 min, some liver slices were incubated in PBS containing glucose at different concentrations (0, 100, or 400 mg dL^{-1}) at 37 °C. Then, time-lapse imaging was performed using CLSM. The integrated densities of images at different time points were quantified using ImageJ. Taking the integrated density at the start of the experiment (0 min) as 1, the relative integrated densities at 15 and 30 min were calculated. The integrated density changes in the PBS group were ascribed to the quenching of FITC-Ins. After subtracting the values of Pep-PMS in PBS, the relative integrated densities of Pep-PMS at low or high glucose concentrations were obtained.

In Vivo Glucose-Responsive Release Studies on Diabetic Mice: Diabetic mice were fasted overnight before the experiment. Pep-PMS were prepared by loading with insulin, GOx, IR 783, and TQ7. First, the mice were subcutaneously injected with an insulin solution at a dose of 5 IU kg^{-1} to lower the blood glucose, and then Pep-PMS (70 mg kg^{-1}) were orally administered. At 2 and 6 h after administration of Pep-PMS, a glucose solution was administered by intraperitoneal injection at a dose of 1.5 g kg^{-1}. The mouse was anesthetized using isoflurane and visualized by the IVIS system at various time points.

In Vivo PD and PK Studies: Diabetic rats were fasted overnight before experiments but allowed free access to water, thus making the gastrointestinal tract clean which do not contain glucose. Ins, insulin-loaded PMS, and Pep-PMS were administered at a dose of 100 IU kg^{-1} in a volume of 2 mL via gavage. Free insulin solution was also administered at a dose of 5 IU kg^{-1} via subcutaneous injection. At 6 h post administration, a glucose solution was administered via gavage at a dose of 2 g kg^{-1} to the Pep-PMS group. Blood samples were collected from the tail veins of rats prior to drug administration and at distinct time intervals after dosing. The blood glucose levels were determined using a glucose meter. For analysis of peripheral serum insulin levels, blood samples were centrifuged at 1800 g for 5 min, and the serum was incubated with high glucose solution for 12 h. Then, the peripheral serum insulin concentration was quantified using a human insulin ELISA kit (Mercodia, Sweden). The area under the peripheral serum insulin concentration versus time curve (AUC) was calculated for each group. The relative bioavailability (*F* %) of test PMS after oral administration was calculated using the following formula

$$F\% = \frac{AUC_{oral} \times Dose_{sc}}{AUC_{se} \times Dose_{oral}} \times 100\% \qquad (1)$$

For analysis of portal serum insulin levels, diabetic rats were administered either Ins, insulin-loaded PMS, or Pep-PMS at a dose of 100 IU kg^{-1} via gavage, and then blood samples were collected from the portal vein by cannulation. The samples were centrifuged at 1800 g for 5 min, and the serum was incubated with high glucose medium for 12 h. Then, the portal serum insulin concentration was quantified using a human insulin ELISA kit. The area under the portal serum insulin concentration versus time curve was calculated for each group.

In Vivo ^{18}F-FDG Uptake in the Liver: Diabetic rats were fasted overnight before experiments but allowed free access to water. The rats were treated with subcutaneous injection of insulin (5 IU kg^{-1}) or orally administered Pep-PMS (100 IU kg^{-1}) 2 h before ^{18}F-FDG administration. The untreated diabetic rats were taken as negative control. Then a glucose solution (2 g kg^{-1}) containing ^{18}F-FDG (18.5 MBq) was orally administered to all diabetic rats. For the Ins-sc group, insulin (5 IU kg^{-1}) was administered again through subcutaneous injection following the ^{18}F-FDG administration. PET and CT scans were performed at 2 h after treatment using an Inveon PET/CT instrument (Siemens, Germany). ^{18}F-FDG PET and CT images were fused using Inveon Research Workplace software. Also, the quantitative SUV-bw values were measured by the software.

Hepatic Glycogen Measurement: Diabetic rats were fasted overnight before experiments but allowed free access to water. The rats were treated with subcutaneous injection of insulin (5 IU kg^{-1}) before each meal or orally administered with Pep-PMS (150 IU kg^{-1}) before the first meal of every day. The untreated diabetic rats were taken as negative control. All rats were fed with standard food every 5 h and three times a day. After provided for 1 h, the food was deprived again. Finally, the rats were sacrificed 2 h after the last meal of 1, 2, and 3 days. The livers were harvested immediately and the hepatic glycogen contents were measured by a glycogen assay kit (Solarbio Science and Technology, China) according to the manual.

Statistical Analysis: All data were directly collected without any processing. All data were presented as mean ± standard deviations (SD). The sample size was three if not specified. All statistical analyses were performed using two-tailed Student's *t* test when two groups were compared, or one-way analysis of variance (ANOVA) with Tukey's post-hoc test when multiple groups were compared in GraphPad Prism 7.0 software. The differences were considered statistically significant for *p* values < 0.05.

Supporting Information

Supporting Information is available from the Wiley Online Library or from the author.

Conflict of Interest

The authors declare no conflict of interest.

Keywords

[1] P. H. Bennett, *Lancet* **2018**, *391*, 2392.

[2] C. Y. Wong, H. Al-Salami, C. R. Dass, *J. Controlled Release* **2017**, *264*, 247.

[3] V. T. Samuel, G. I. Shulman, *Cell Metab.* **2018**, *27*, 22.

[4] a) M. D. Michael, R. N. Kulkarni, C. Postic, S. F. Previs, G. I. Shulman, M. A. Magnuson, C. R. Kahn, *Mol. Cell* **2000**, *6*, 87; b) R. Herring, R. H. Jones, D. L. Russell-Jones, *Diabetes, Obes. Metab.* **2014**, *16*, 1.

[5] M. Stadler, M. Krssak, D. Jankovic, C. Gobl, Y. Winhofer, G. Pacini, M. Bischof, M. Haidinger, M. Saemann, F. Muhlbacher, M. Korbonits, S. M. Baumgartner-Parzer, A. Luger, R. Prager, C. H. Anderwald, M. Krebs, *Clin. Endocrinol.* **2014**, *80*, 208.

[6] a) X. Li, S. Guo, C. Zhu, Q. Zhu, Y. Gan, J. Rantanen, U. L. Rahbek, L. Hovgaard, M. Yang, *Biomaterials* **2013**, *34*, 9678; b) X. Zhang, J. Qi, Y. Lu, W. He, X. Li, W. Wu, *Nanomedicine* **2014**, *10*, 167; c) W. Shan, X. Zhu, M. Liu, L. Li, J. Zhong, W. Sun, Z. Zhang, Y. Huang, *ACS Nano* **2015**, *9*, 2345; d) X. Zhu, J. Wu, W. Shan, W. Tao, L. Zhao, J. M. Lim, M. D'Ortenzio, R. Karnik, Y. Huang, J. Shi, O. C. Farokhzad, *Angew. Chem., Int. Ed. Engl.* **2016**, *55*, 3309; e) M. Alibolandi, F. Alabdollah, F. Sadeghi, M. Mohammadi, K. Abnous, M. Ramezani, F. Hadizadeh, *J. Controlled Release* **2016**, *227*, 58; f) J. Yu, Y. Zhang, J. Wang, D. Wen, A. R. Kahkoska, J. B. Buse, Z. Gu, *Nano Res.* **2019**, *12*, 1539; g) H. Tian, Z. He, C. Sun, C. Yang, P. Zhao, L. Liu, K. W. Leong, H. Q. Mao, Z. Liu, Y. Chen, *Adv. Healthcare Mater.* **2018**, *7*, e1800285.

[7] a) D. W. Acheson, R. Moore, S. De Breucker, L. Lincicome, M. Jacewicz, E. Skutelsky, G. T. Keusch, *Infect. Immun.* **1996**, *64*, 3294; b) Y. Hirakata, K. Izumikawa, T. Yamaguchi, S. Igimi, N. Furuya, S. Maesaki, S. Tomono, Y. Yamada, S. Kohno, K. Yamaguchi, S. Kamihira, *Infect. Immun.* **1998**, *66*, 1748; c) A. L. Daugherty, M. L. McKee, D. J. FitzGerald, R. J. Mrsny, *J. Controlled Release* **2000**, *65*, 297.

[8] W. I. Lencer, S. Moe, P. A. Rufo, J. L. Madara, *Proc. Natl. Acad. Sci. U. S. A.* **1995**, *92*, 10094.

[9] E. Valerio, S. Chaves, R. Tenreiro, *Toxins* **2010**, *2*, 2359.

[10] Q. Wu, L. Wang, H. Yu, J. Wang, Z. Chen, *Chem. Rev.* **2011**, *111*, 7855.

[11] J. Yang, Z. Cao, *J. Controlled Release* **2017**, *263*, 231.

[12] a) J. Yu, Y. Zhang, Y. Ye, R. DiSanto, W. Sun, D. Ranson, F. S. Ligler, J. B. Buse, Z. Gu, *Proc. Natl. Acad. Sci. U. S. A.* **2015**, *112*, 8260; b) X. Hu, J. Yu, C. Qian, Y. Lu, A. R. Kahkoska, Z. Xie, X. Jing, J. B. Buse, Z. Gu, *ACS Nano* **2017**, *11*, 613; c) J. Yu, C. Qian, Y. Zhang, Z. Cui, Y. Zhu, Q. Shen, F. S. Ligler, J. B. Buse, Z. Gu, *Nano Lett.* **2017**, *17*, 733.

[13] a) J. M. Gamboa, K. W. Leong, *Adv. Drug Delivery Rev.* **2013**, *65*, 800; b) L. Zheng, C. J. Kelly, S. P. Colgan, *Am. J. Physiol. Cell Physiol.* **2015**, *309*, C350.

[14] T. Matsubara, D. Ishikawa, T. Taki, Y. Okahata, T. Sato, *FEBS Lett.* **1999**, *456*, 253.

[15] a) W. Tai, R. Mo, J. Di, V. Subramanian, X. Gu, J. B. Buse, Z. Gu, *Biomacromolecules* **2014**, *15*, 3495; b) N. K. Singh, D. S. Lee, *J. Controlled Release* **2014**, *193*, 214; c) C. He, X. Zhuang, Z. Tang, H. Tian, X. Chen, *Adv. Healthcare Mater.* **2012**, *1*, 48; d) H. Lu, J. Wang, Z. Song, L. Yin, Y. Zhang, H. Tang, C. Tu, Y. Lin, J. Cheng, *Chem. Commun.* **2014**, *50*, 139.

[16] a) G. Li, C. Zhao, X. Li, D. Qi, C. Liu, F. Bu, H. Na, *Polym. Chem.* **2015**, *6*, 5911; b) A. Napoli, M. Valentini, N. Tirelli, M. Muller, J. A. Hubbell, *Nat. Mater.* **2004**, *3*, 183.

[17] D. E. Discher, F. Ahmed, *Annu. Rev. Biomed. Eng.* **2006**, *8*, 323.

[18] a) J. M. Harris, R. B. Chess, *Nat. Rev. Drug Discovery* **2003**, *2*, 214; b) C. Y. Sun, S. Shen, C. F. Xu, H. J. Li, Y. Liu, Z. T. Cao, X. Z. Yang, J. X. Xia, J. Wang, *J. Am. Chem. Soc.* **2015**, *137*, 15217.

[19] A. R. Rodriguez, J. R. Kramer, T. J. Deming, *Biomacromolecules* **2013**, *14*, 3610.

[20] a) L. M. Ensign, R. Cone, J. Hanes, *Adv. Drug Delivery Rev.* **2012**, *64*, 557; b) M. Yu, J. Wang, Y. Yang, C. Zhu, Q. Su, S. Guo, J. Sun, Y. Gan, X. Shi, H. Gao, *Nano Lett.* **2016**, *16*, 7176; c) M. Yu, L. Xu, F. Tian, Q. Su, N. Zheng, Y. Yang, J. Wang, A. Wang, C. Zhu, S. Guo, X. Zhang, Y. Gan, X. Shi, H. Gao, *Nat. Commun.* **2018**, *9*, 2607.

[21] a) P. Y. Lin, E. Y. Chuang, Y. H. Chiu, H. L. Chen, K. J. Lin, J. H. Juang, C. H. Chiang, F. L. Mi, H. W. Sung, *J. Controlled Release* **2017**, *259*, 168; b) H. Pang, P. U. Le, I. R. Nabi, *J. Cell Sci.* **2004**, *117*, 1421.

[22] a) A. Melkoumov, I. St-Jean, X. Banquy, G. Leclair, J. Leblond Chain, *Mol. Pharmaceutics* **2019**, *16*, 60; b) D. E. Saslowsky, Y. M. te Welscher, D. J. Chinnapen, J. S. Wagner, J. Wan, E. Kern, W. I. Lencer, *J. Biol. Chem.* **2013**, *288*, 25804.

[23] W. Fan, D. Xia, Q. Zhu, L. Hu, Y. Gan, *Drug Discovery Today* **2016**, *21*, 856.

[24] a) Y. Uchida, J. Hasegawa, D. Chinnapen, T. Inoue, S. Okazaki, R. Kato, S. Wakatsuki, R. Misaki, M. Koike, Y. Uchiyama, S. Iemura, T. Natsume, R. Kuwahara, T. Nakagawa, K. Nishikawa, K. Mukai, E. Miyoshi, N. Taniguchi, D. Sheff, W. I. Lencer, T. Taguchi, H. Arai, *Proc. Natl. Acad. Sci. U. S. A.* **2011**, *108*, 15846; b) W. I. Lencer, B. Tsai, *Trends Biochem. Sci.* **2003**, *28*, 639.

[25] Y. N. Zhang, W. Poon, A. J. Tavares, I. D. McGilvray, W. C. W. Chan, *J. Controlled Release* **2016**, *240*, 332.

[26] V. T. Samuel, G. I. Shulman, *J. Clin. Invest.* **2016**, *126*, 12.

[27] a) K. Itaka, T. Ishii, Y. Hasegawa, K. Kataoka, *Biomaterials* **2010**, *31*, 3707; b) A. Banerjee, K. Ibsen, T. Brown, R. Chen, C. Agatemor, S. Mitragotri, *Proc. Natl. Acad. Sci. U. S. A.* **2018**, *115*, 7296.

[28] J. R. Kramer, T. J. Deming, *Biomacromolecules* **2010**, *11*, 3668.

[29] Y. Bi, L. Liu, Y. Lu, T. Sun, C. Shen, X. Chen, Q. Chen, S. An, X. He, C. Ruan, Y. Wu, Y. Zhang, Q. Guo, Z. Zheng, Y. Liu, M. Lou, S. Zhao, C. Jiang, *ACS Appl. Mater. Interfaces* **2016**, *8*, 27465.

[30] W. Fan, D. Xia, Q. Zhu, X. Li, S. He, C. Zhu, S. Guo, L. Hovgaard, M. Yang, Y. Gan, *Biomaterials* **2018**, *151*, 13.

[31] F. Y. Su, K. J. Lin, K. Sonaje, S. P. Wey, T. C. Yen, Y. C. Ho, N. Panda, E. Y. Chuang, B. Maiti, H. W. Sung, *Biomaterials* **2012**, *33*, 2801.

[32] C. Damge, P. Maincent, N. Ubrich, *J. Controlled Release* **2007**, *117*, 163.

[33] I. A. de Graaf, P. Olinga, M. H. de Jager, M. T. Merema, R. de Kanter, E. G. van de Kerkhof, G. M. Groothuis, *Nat. Protoc.* **2010**, *5*, 1540.